
# Visualization of delayed release of compounds from pH-sensitive capsules in vitro and in vivo in a hamster model


| | |
|---|---|
| Journal: | *Contrast Media and Molecular Imaging* |
| Manuscript ID: | CMMI-14-0081.R1 |
| Wiley - Manuscript type: | Full Paper |
| Date Submitted by the Author: | n/a |



| | |
|---|---|
| Complete List of Authors: | Staelens, Dominiek; University of Leuven, Translational Research Center for Gastrointestinal Disorders, Department of Clinical and Experimental Medicine<br>Liang, Sayuan; University of Leuven, Biomedical MRI, MoSAIC, Department of Imaging and Pathology<br>Appeltans, Bernard; University of Leuven, Laboratory of Drug Delivery and Disposition, Department of Pharmaceutical and Pharmacological Sciences<br>Van de Wouwer, Marlies; University of Leuven, Laboratory for Therapeutic and Diagnostic Antibodies; Department of Pharmaceutical and Pharmacological Sciences; University of Leuven, PharmAbs<br>Van den Mooter, Guy; University of Leuven, Laboratory of Drug Delivery and Disposition, Department of Pharmaceutical and Pharmacological Sciences<br>Van Assche, Gert; University of Leuven, Translational Research Center for Gastrointestinal Disorders, Department of Clinical and Experimental Medicine<br>Himmelreich, Uwe; University of Leuven, Biomedical MRI, MoSAIC, Department of Imaging and Pathology<br>Vande Velde, Greetje; University of Leuven, Biomedical MRI, MoSAIC, Department of Imaging and Pathology |



| | |
|---|---|
| Keyword: | Controlled release, 19F-MRI, CT, in vivo, multimodal imaging, pH-sensitive capsules |

**Title:** Visualization of delayed release of compounds from pH-sensitive capsules *in vitro* and *in vivo* in a hamster model

**Short title:** Combined CT and $^{19}$F-MR imaging for visualization of delayed release

Dominiek Staelens[1,*], Sayuan Liang[2,*], Bernard Appeltans[3], Marlies Van de Wouwer[4,5], Guy Van den Mooter[3], Gert Van Assche[1], Uwe Himmelreich[2,*], Greetje Vande Velde[2,*]

[1]Translational Research Center for Gastrointestinal Disorders, Department of Clinical and Experimental Medicine, KU Leuven, Leuven, Belgium

[2]Biomedical MRI unit/ MoSAIC, Department of imaging and pathology, KU Leuven, Leuven, Belgium

[3]Drug Delivery and Disposition, Department of pharmaceutical and pharmacological sciences, KU Leuven, Leuven, Belgium

[4]Laboratory for Therapeutic and Diagnostic Antibodies, Department of Pharmaceutical and Pharmacological Sciences, KU Leuven, Leuven, Belgium

[5]PharmAbs, KU Leuven, Leuven, Belgium

[*] Authors contributed equally.

**Correspondence:**

Greetje Vande Velde, O&N I, Herestraat 49 – Box 505, 3000 Leuven, Belgium;
tel. +32 16 3 30924 fax +32 16 3 30901; e-mail
greetje.vandevelde@med.kuleuven.be

Uwe Himmelreich, O&N I, Herestraat 49 – Box 505, 3000 Leuven, Belgium;
tel. +32 16 3 30925; fax +32 16 3 30901; e-mail
uwe.himmelreich@med.kuleuven.be

**Keywords** Controlled release, $^{19}$F-MRI, CT, *in vivo*, multimodal imaging, pH-sensitive capsules

**Acknowledgement:** This work was supported by grants from the agency for Innovation by Science and Technology (IWT/100548, IWT 130065 (SBO MIRIAD) and IWT 140061 (SBO NanoCoMIT)), the European Commission MC ITN Betatrain (289932) and the KU Leuven program financing IMIR (PF 2010/017). GVV is a postdoctoral fellow of the Research Foundation Flanders (FWO) and GVA is a senior clinical researcher of the FWO.

## Abstract

Delayed controlled release is an innovative strategy to locally administer therapeutic compounds (e.g. chemotherapeutics, antibodies etc.). This would improve efficiency and reduce side effects compared to systemic administration. To enable the evaluation of the efficacy of controlled release strategies both *in vitro* and *in vivo*, we investigated the release of contrast agents ($^{19}$F-FDG and $BaSO_4$) to the intestinal tract from capsules coated with pH-sensitive polymers (Eudragit L-100) by using two complementary techniques, *i.e.* $^{19}$F magnetic resonance imaging (MRI) and computed tomography (CT).

Using *in vitro* $^{19}$F-MRI, we were able to non-destructively and dynamically establish a time window of two hours during which the capsules are resistant to low pH. With $^{19}$F-MRI, we could establish the exact time point when the capsules became water permeable, before physical degradation of the capsule. This was complemented by CT imaging that provided longitudinal information on physical degradation of the capsule at low pH that was only seen after 230 minutes. After oral administration to hamsters, $^{19}$F-MRI visualized the early event whereby the capsule becomes water permeable after 2 hours. Additionally, using CT, the integrity and location (stomach and small intestines) of the capsule after administration could be monitored.

In conclusion, we propose combined $^{19}$F-MRI and CT to non-invasively visualize the different temporal and spatial events regarding the release of compounds, both in an *in vitro* setting as in the gastrointestinal tract of small animal models. This multimodal imaging approach will enable the *in vitro* and *in vivo* evaluation of further technical improvements to controlled release strategies.

## Introduction

Controlled release of therapeutic compounds at the disease location is a strategy that aims for a local effect and more precise targeting of pathological processes. It is anticipated that oral administration and delivery of therapeutic compounds directly inside the intestine (also called luminal delivery) can have considerable advantages over systemic administration. These include lower concentrations of drug needed, which reduces costs and lowers systemic side effects (1). One example where targeted delivery to the gastrointestinal tract could improve outcome is the controlled and localized release of antibodies targeting virulence factors against *Clostridium difficile* associated disease, which accounts for 71% of gastrointestinal nosocomial infections, but has currently a cure rate of only 70% with standard systemic administration of antibiotics (2-5).

This situation and other clinical settings may benefit from an approach where therapeutic compounds are enclosed within a capsule for oral administration, designed to release its content only when it reaches its target location, in this case the small intestine. The pH in the human gastrointestinal tract increases progressively from the stomach (pH 2-3), the small intestine (pH 6.5-7) to the colon (pH 7-7.8) (6), with intra- and inter-individual differences. This makes it possible to coat a capsule with a polymer that is resistant to low pH and thus passes the stomach and dissolves at increased pH in a specific part of the gastrointestinal tract. Targeted drug release by capsules coated with pH-sensitive materials has been described for a wide variety of cases (7). A rise in pH induces dissolution or swelling of the polymers, thereby leading to a disruption of the capsule coating, resulting in the release of its content (8).

Delivery of a drug inside the gastrointestinal tract can be analyzed with a variety of techniques including enzyme-linked immunosorbent assay and mass spectrometry on luminal content (9,10). Nevertheless, these techniques have the disadvantage that animals need to be sacrificed for sample collection. Moreover, these approaches only provide snapshot data on the location and physical integrity of the capsule at the moment of sacrifice, and lack information on

compound release. The existing non-invasive option, i.e. measuring drug levels in fecal samples, lacks information on the exact site of release. To validate and optimize controlled release strategies and enable translational studies evaluating these novel therapeutic approaches, there is the need for a sensitive, non-invasive method to longitudinally evaluate capsule integrity, the anatomical location and the (early) release of compounds.

Different medical imaging modalities have been applied frequently in both clinical and pre-clinical research providing new perspectives for biomedical research (11). Despite differences in resolution, sensitivity, penetration and safety, the main advantage of imaging techniques is that they provide non-invasive, non-destructive and direct information both *in vitro* and *in vivo*. As such, gamma scintillation is frequently used as an imaging technique in clinical research for controlled release studies (12,13). It offers good sensitivity and a relatively simple procedure for acquiring images to follow capsule movement by means of a radioactive tracer that is included in the capsule just before administration. A potential concern with this technique is the need of gamma emitting radionuclides, which may hinder longitudinal monitoring due to their restricted half-lives and involve possible safety issues. Furthermore, the low resolution and the lack of anatomical background information make it difficult to interpret the images. Alternatively, endoscopy has also been applied for direct visualization of intraluminal drug delivery studies in humans (14). Although this technique could provide direct information regarding time and place of capsule rupture, dispersion characteristics and the surrounding physiological environment, the investigation with the large encapsulated camera is intrusive and offers only a limited field of view.

In a preclinical research context, there is even more need for a sensitive, non-invasive approach to evaluate controlled release in the 3D-context of the animal's anatomy. MRI and CT are valuable imaging modalities, employed in a wide range of studies thanks to their ability to provide 3D anatomical images with excellent resolution and without the need for radioactive tracers (11). Especially MRI has been employed in pharmaceutical studies as it is devoid of

any ionizing radiation (15,16). Due to its relatively low sensitivity, conventional contrast agents such as superparamagnetic iron oxide and paramagnetic gadolinium/manganese are frequently used to enhance the contrast against the background (17-19). However, the contrast generated by those agents is not directly quantifiable and not always unambiguous due to similar intrinsic contrast changes, in particular in the abdomen. This can be overcome by the use of $^{19}$F-containing contrast agents. These have shown to be complementary to the acquisition of traditional proton-based, anatomical images ($^{1}$H-MRI) (20). Due to the lack of MR-detectable $^{19}$F signal inside biological tissues, all signal from $^{19}$F-MRI origins from the (dissolved) contrast agent, which makes the technique very specific and quantifiable (21). In this study, 2-fluoro-2-deoxy-D-glucose ($^{19}$F-FDG) is used as contrast agent for $^{19}$F-MRI as it is only MR-detectable when dissolved in water and, as a glucose analog, is considered to be safe (22). On the other hand, barium sulphate ($BaSO_4$), based on the high atom-number and hence high x-ray absorption of barium, is used as a CT contrast agent for gastrointestinal tract imaging to increase the contrast between the gastrointestinal contents compared to the surrounding soft tissues (23,24). Moreover, $BaSO_4$ can be safely used for oral administration because of the absence of toxicity (25).

By loading the pH-sensitive capsules with both contrast agents and by combining CT and $^{19}$F MRI, we hypothesized that the $^{19}$F-MRI FDG signal would provide information on early permeability of the capsule material to water and its location, while the $BaSO_4$ contrast and the CT images can be used to monitor capsule integrity and the exact anatomical location of the site of release.

In this study, we evaluated the ability of this dual imaging approach as a tool to evaluate the resistance of coated capsules at different pHs *in vitro* and *in vivo* after oral administration to hamsters. The objective is to combine different imaging modalities to non-destructively and longitudinally visualize and explore the kinetics of controlled release under different conditions.

## Results and Discussion

*In vitro imaging*

In a first set of experiments, we conducted *in vitro* studies to investigate the resistance of coated capsules at different levels of acidity (pH = 1, 3, 5 and 7) with both MRI and CT (figure 1 and 2, respectively). For MR imaging, the $^{19}F$ signal was overlaid with the anatomical $^{1}H$ image. At the first time point, one hour after the capsule was added to the solutions, the capsules at pH 5 and 7 showed quantifiable $^{19}F$-FDG signal (figure 1A). This indicates that the surrounding solution enters into the capsule and dissolves some of the otherwise not visible, encapsulated $^{19}F$-FDG, which was then picked up by $^{19}F$-MRI. This is in contrast to the capsules at low pH (pH 1 and 3), where the $^{19}F$-MRI signal could only be seen after one hour and a half (figure 1D), which indicates that the coating has more resistance at lower pH than at higher pH. In the timeframe of 2-4 hours, for the capsules at all pHs, maximal signal intensity was reached, albeit at different time points (figure 1B and D). The time point at which the maximal signal intensity was reached, depended on the extra-capsular pH. The lower the pH, the longer the time needed to fully dissolve the $^{19}F$-FDG (figure 1D). In general, the $^{19}F$-MRI signal was first limited to the area of the actual capsule, indicating that although the $^{19}F$-FDG inside the capsule was dissolved, the exchange with the extra-capsular space was slow. After the $^{19}F$-FDG peak intensity reached a maximum, the signal gradually decreased (figure 1D). This process could be explained by the gradual diffusion of the $^{19}F$-FDG outside the capsule, which was confirmed by a rise in signal intensity observed in a MRI slice outside the capsule but inside the microcentrifuge tube (figure 1E). Later, this process is further accelerated by the degradation of the capsule. The signal intensity ratio between the intra- and extra-capsular spaces reached an equilibrium after 8-10 hours (depending on the pH). A macroscopic examination of the phantom after the MRI session confirmed that the capsules were degraded and their content dissolved.

More information about the structure of the capsule with higher spatial and temporal resolution was acquired by performing CT of capsules containing

$BaSO_4$ (figure 2). The time span of the longitudinal scans that were acquired from the same material as for the MRI experiments was limited to 8 hours. The results of the CT imaging clearly showed the degradation of the capsule after 230 minutes in pH 5 and 7. The red arrowheads in figure 2 indicate the site of the capsule where degradation was first observed. This confirms the observation that the coated capsules are resistant to low pH. The physical degradation could be clearly visualized leading to the loss of contrast from the capsule material (see arrows in figure 2). The degradation of the capsule coincided with the accumulation of $BaSO_4$ on the bottom of the microcentrifuge tube. Based on these results, CT imaging provides additional information about the later event of physical capsule degradation after the early increased permeability that was observed by MRI. The fact that there is no clear difference between the timing of degradation at pHs 5 and 7 does not conflict with the strategy to achieve a controlled release upon transit through the stomach, which normally has a lower pH. A complete degradation of all capsules at pH 1 was only observed after 400 minutes.

Based on the data acquired from the *in vitro* assessment of the low pH resistance of the coated capsules, we showed that MRI and CT result in complementary data regarding both permeability of the capsule to water and degradation of the capsule. Moreover, we demonstrated the resistance against low pH for up to 2 hours by MRI and CT, which overcomes the normal transit time of the stomach (26).

*In vivo imaging*

In a next set of experiments, we longitudinally monitored capsules containing both $^{19}$F-FDG and $BaSO_4$ using *in vivo* MRI and CT after oral administration to hamsters. In all animals, a clear $^{19}$F-MRI signal was observed in the stomach 2 hours after administration (figure 3A-C). The extent of the detected $^{19}$F-MRI signal was within the range of the physical size of the capsule based on the $^{1}$H-MR images. This indicates that fluid from the stomach entered into the capsule and dissolved the $^{19}$F-FDG. However, the capsule was not disintegrated. This is in line with the *in vitro* results. Figure 3D shows that after 5 hours, there was no

detectable $^{19}$F-MRI signal due to the degradation of the capsule leading to the release of $^{19}$F-FDG from the capsule and further dilution of the $^{19}$F-MRI signal below the detectability threshold. Non-localized *in vivo* $^{19}$F NMR spectra of the abdominal cavity show similar signal amplitudes at these two time points, which confirmed that the total amount of $^{19}$F -FDG inside the animal remains at a similar level but is no longer entirely localized in the capsule after 5 hours (figure 3E). The $^{19}$F NMR spectra in figure 3E were generated by using a non-localized single pulse sequence instead of the localized PRESS sequence to cover the whole field of view. Quantification of the $^{19}$F-signal normalized to the signal at the 2 hour time point confirms almost constant signal intensity (100 % vs 97 %, insert in figure 3E).

CT of the same capsule and animal was also used for the localization of the capsule and the assessment of the integrity of the capsule (figure 4). The $BaSO_4$-containing capsule was clearly visible in the stomach right after administration, even from a 2D, non-reconstructed projection image (figure 4A). The early events of increased permeability of the capsule, as was seen by $^{19}$F-MRI, could not be visualized by CT. On the other hand, a clear degradation of the capsule and the release of the mainly non-dissolved $BaSO_4$-content into the stomach were observed after 6 hours (figure 4B-D). CT using $BaSO_4$ gives anatomical information with good sensitivity and high resolution both spatially and temporally. It provides positive contrast from the beginning until the degradation of the capsule and enables imaging of release of the solid capsule content into the gastrointestinal tract. The insolubility of barium salts has particularly the advantage that the contrast agent is trapped in the gastrointestinal tract resulting in reduced toxicity.

The *in vivo* findings verify our *in vitro* results that the coated capsule could resist the low pH environment of the stomach without degradation for at least two hours. During this time, the location and integrity of the capsule can be monitored with CT, for both cases where the capsule remains trapped in the stomach for 6 hours (3 out of 4 hamsters tested), or passes the stomach and reached the small intestine (1 observation), 3 hours after administration (figure

5), consistent with previous studies in rats regarding capsule size and gastric retention (24,27). When $^{19}$F-FDG is dissolved, diffused out of the capsule and taken up by cells/ in the blood stream, it leads to the loss of a clearly localized $^{19}$F-MRI signal (figure 5A). The feeding status of animals is a known factor that influences the transit of capsules (24). In our study, all animals were in a fed state. Another important aspect is the time during the day (activity vs. resting phase) when the capsule was administered. In this study, hamsters were dosed with the capsules during the light cycle. However, we did not observe any difference in transit time when the capsules were administered during the dark cycle (n=2, data not shown).

The dual-modal imaging approach proposed in this study could in principle be applied to any other studies of controlled release from capsule material as both CT and MRI are readily available in modern clinical and pre-clinical environments for routine diagnosis and research purpose. Barium sulfate enhanced CT has already been used for gastrointestinal tract imaging to increase the contrast between the gastrointestinal contents compared to the surrounding soft tissues (24) due to the high atom-number and hence high x-ray absorption of barium. Furthermore, barium sulfate can also be safely used for oral administration because of the absence of toxicity (25).

On the other hand, to the best of our knowledge, this is the first time that $^{19}$F-MRI was applied for controlled release studies from capsule material in an animal model. Thanks to its high specificity and quantitative feature, $^{19}$F-MRI used in this study provides detailed information to better understand the early events of capsule degradation, starting with an increase in permeability leading to an influx of liquids. Due to the relatively low sensitivity of MRI and the relatively low concentrations of $^{19}$F-FDG, $^{19}$F-MRI as applied in our study has only a temporal resolution in the order of 30 minutes and does not provide information on the capsule itself once the $^{19}$F-FDG has been released. Optimization of the magnetic resonance pulse sequence could be a key to reduce the scan time. This was shown to result in similar signal-to-noise ratio but reduced scan time, which should be further explored by analyzing the characteristics of $^{19}$FDG (20).

Recently, compressed sensing is also considered a reliable reconstruction technique to speed up the MRI scanning. According to Zhong *et al.*, by under-sampling the k-space factor of 8, compressed sensing could still retrieve the image with a similar signal-to-noise-ratio (28). Other methods including different coil set-ups and higher field strength could also be considered as potential ways to improve the sensitivity of the technique, reducing scan time and thus improving temporal resolution. The $^{19}$F-MRI technique could potentially be applied for clinical use as clinical trials have already been carried out by using perfluorocarbons (4). The safety of fluorodeoxyflucose at physiological concentrations has been demonstrated by its frequent use as a tracer for positron emission tomography in the clinic (29). Higher FDG concentrations used for $^{19}$F MRI have not yet been assessed from a toxicological point of view. However, some pre-clinical studies did not indicate any adverse effects (22).

Based on our proof-of-principle data, a future step will be to evaluate a pH-controlled delivery in the gastrointestinal tract of antibodies against *C. difficile* by a pH-sensitive polymer coated capsule. Our dual-modality imaging approach enabled us to evaluate *in vivo* both the location and integrity of the capsule. As antibodies are generally well soluble, we would anticipate that they will distribute similar to the FDG used in our study. In order to test antibody release in the hamster model, parameters like different capsule sizes or capsule coating have to be further optimized for their ability to pass the stomach. By reducing the size of the capsule or modifying capsule coating to withstand low pH for longer, we expect the success rate to increase.

## Conclusions

We were able to show that combined application of $^{19}$F-MRI and CT provides information on the location, integrity and graduate release of material from oral administered capsules into the gastrointestinal tract of small animal models. This will form the basis for further studies on the delivery of therapeutic compounds, *e.g.* antibodies against *Clostridium difficile* infection.

Both imaging modalities provide complementary information about the position and release of contrast agents (or drugs) inside the gastrointestinal tract. CT was shown to be useful for monitoring the localization of the capsule as well as the integrity of it. On the other hand, $^{19}$F-MRI enabled the visualization of the rise in permeability of the capsule. A $^{19}$F-MRI signal could only be detected when $^{19}$F-FDG was dissolved and this happened when there was influx of water into the capsule. Furthermore, it should be noted that the degree of compound release is influenced by the solubility of the compound itself. For example, lyophilized antibodies can be stable and are well solubilized. As an intermediate step in the development of the oral administration of encapsulated antibodies, we envisage capsules to be filled with both, $^{19}$F-FDG and $BaSO_4$ as well as the antibody. In that way the controlled release can be monitored non-invasively.

Overall, we have proposed and demonstrated an imaging platform to monitor the mechanism of controlled release *in vitro* and *in vivo*. This multimodal platform could overcome the limitations in terms of sensitivity, resolution, specificity and quantitation of one individual method. We believe that this imaging approach could also be applied to other models where controlled release mechanisms need to be understood and evaluated.

## Experimental

*Capsules and contrast agents*

Gelatin size 9 capsules (8.4 mm in length, 2.7 mm external diameter and 25 µl maximal volume, Torpac, Fairfield, USA) were filled with FDG and/or $BaSO_4$ (average amounts were 3.63 mg (equal to 20 µmol) and 14.49 mg (equal to 62 µmol), respectively). Afterwards, the capsules were dip-coated with a solution of 12.5% Eudragit L100 (Evonik Industries, Essen, Germany) in isopropanol. Triethylcitrate (10% w/w) was added as plasticizer.

*Hamster model*

All animal experiments were executed in accordance with national and European regulations and approved by the Animal Ethics Committee of the KU Leuven (approval numbers P009/2010 and P083/2011). Four male Syrian Golden hamsters (120-150 g, Janvier Laboratories) were given capsules via oral gavage using a dosing syringe (Torpac, Fairfield, USA). All animals were dosed and imaged during the light cyclus while being in a fed *ad libitum*. Additional experiments were performed whereby two animals were dosed and imaged during the dark cyclus but this did not impact the results discussed here (data not shown).

*Magnetic Resonance Imaging*

MRI was carried out on a 9.4 Tesla Bruker Biospec small animal MR scanner (Bruker Biospin, Ettlingen, Germany; horizontal bore, 20cm) equipped with actively shielded gradients (600 mT $m^{-1}$) and running under the operating system ParaVision 5.1. For radiofrequency transmission and reception, a home-built, inductively coupled, saddle shaped surface coil, tunable from 376 MHz for $^{19}F$ to 400 MHz for $^{1}H$ was used for all experiments.

For *in vitro* MRI, a phantom was prepared by filling 2% agarose in a plastic container containing 4 microcentrifuge tubes (Eppendorf, Hamburg, Germany). Each tube contained 400 µl PBS with different pH (pH = 1, 3, 5 and 7) adjusted by adding HCl (1M). In each tube, one intact capsule loaded with $^{19}F$-FDG was added. A positioning and anatomic $^{1}H$-MRI scan was performed using a 2D turbo

spin echo sequence (RARE sequence, 8 echoes/excitation, 7.6 s/15.9 ms repetition time/effective echo time, 6.4 cm*6.4 cm field of view, 256*256 matrix, 100 consecutive, coronal, 0.25 mm slice thickness, number of average is 2, 6 min scanning time). The settings for non-localized $^{19}$F-NMR spectroscopy were: 100 ms repetition time, 1000 numbers of average, flip angle of 20° and total scan time of 100 s. $^{19}$F-MRI 2D images were obtained using the same sequence as for $^{1}$H-MRI imaging with some parameters modified (1.142 s repetition time, 64*64 matrix, 15 consecutive 1 mm thick slices in coronal orientation, 250 number of average, 28:30 min scan time). Repeated *in vitro* images were acquired over a period of 15 hours, until the capsules were considered to be totally disintegrated.

For *in vivo* MRI, hamsters were scanned under inhalation anesthesia (1-2% isoflurane mixed with carrier gas oxygen). A monitoring and gating model (type 1030) from SA Instruments Inc. (Stony Brook, NY, USA) was used to regulate the physiological parameters and respiratory gating in real time. The body temperature and respiration rate of animals were monitored using a rectal probe and a pressure sensitive pad placed underneath the thorax, respectively. Both body temperature and respiration rate were maintained at reasonable physiological range of approximately 37°C and 30-50 breaths/min, respectively. Both anatomical images ($^{1}$H-MRI) and $^{19}$F-MR images were acquired using RARE sequences with modified parameters: 15.9 ms effective echo time; 6 s ($^{1}$H)/1 s ($^{19}$F) repetition time, 8 echoes/excitation; 6 cm * 8 cm field of view; 300*400 ($^{1}$H)/50*50 ($^{19}$F) matrix; 50 ($^{1}$H)/10 ($^{19}$F) consecutive, coronal slices of 0.5 mm (for $^{1}$H) and 2.5 mm (for $^{19}$F) thickness; number of averages was 2 for $^{1}$H and 500 for $^{19}$F; scan time was 7:24 min for $^{1}$H and 33:20 min for $^{19}$F. Multiple $^{19}$F MR images were obtained using the same scan protocol. The total scan time was maximum 2.5 hours. The $^{19}$F NMR spectra were analyzed using the Jmri software, version 4.0 (30).

*Computed Tomography*

CT images were acquired on a dedicated small animal microCT scanner (SkyScan 1076, Bruker microCT, Kontich, Belgium), reconstructed and visualized using software provided by the manufacturer (NRecon, DataViewer, CTvox).

*In vitro* microCT phantom scans were acquired using the following scan parameters: 100 kVp X-ray source voltage combined with a 1.0 mm aluminum filter, 100 µA source current, 220 ms exposure time per projection, resulting in a total scan time of less than 7 minutes.

For the acquisition of *in vivo* CT scans, hamsters were anesthetized with 1.5 – 1% isoflurane in 100 % oxygen. Scan parameters were: 50 kVp X-ray source voltage combined with a 0.5 mm aluminum filter, 180 µA source current, 450 ms exposure time per projection, acquiring 2 projections (for averaging) per position with 0.7° increments over a total angle of 180° and a field-of-view covering the stomach and bowels, resulting in a scanning time of 12 minutes. This yielded a reconstructed 3D datasets with 35 $\mu m^3$ isotropic voxel size.

## Figure legends

**Figure 1: *In vitro* $^{19}$F-MRI monitoring.** Coated capsules containing $^{19}$F-FDG in microcentrifuge tubes containing solutions of different pH were monitored for 15 hours by $^{19}$F-MRI. The time to reach the maximum signal intensity depended on the pH in which the capsule was incubated. The $^{19}$F NMR signal was first detectable in the capsules incubated at the highest pH. After three hours, a signal was observed for all capsules incubated within the pH-range 1 to 7. A-C: representative $^{1}$H-MRI slices (gray scale) are overlaid with the corresponding $^{19}$F signal (red-hot scale) after 1 (A), 3 (B) and 15 hours (C) in the solution. The same $^{19}$F-MRI signal intensity threshold was set manually for all images. (D-E): Quantitative $^{19}$F-MRI signal inside (D) and outside (E) the capsule of a representative slice based on the $^{1}$H-MRI image. Time resolution is 30 mins for the different pHs. The signal intensities are normalized to the maximum signal intensity (=100%) of the slice inside the capsule. Signal intensities were retrieved from locations corresponding to the intra-capsular space (D) or from a slice outside the capsule (E).

**Figure 2: *In vitro* CT monitoring.** Coated capsules containing $BaSO_4$ in microcentrifuge tubes containing solutions at different pH (indicated in the figure by 1, 3, 5 and 7) were monitored for 8 hours by CT. Upper row: longitudinal 2D projection images; bottom row: corresponding 3D volume-rendered reconstructed images. Capsule disintegration only occured after 230 min at pH 5 and 7, whereas at pH 1 the capsule only disintegrated after 400 min. Note: all capsules have the same size, the apparent different size between different capsules is due to the 3D rendering viewing angle. The red arrows indicate the site in the capsule where the first clear indication of degradation is observed.

**Figure 3: In vivo MRI monitoring of the $^{19}$F-MR signal in the digestive track of hamsters.** Coated capsules containing $^{19}$F-FDG and $BaSO_4$ were administered to hamsters and subsequently visualized by $^{19}$F-MRI. A: representative $^{1}$H-MR image slice visualizing the stomach; B: corresponding $^{19}$F MR image (grey scale) two hours after oral administration of the capsule (grey scale) and C: composite

of A and B (with the $^{19}$F MR image red-hot scaled with a manually set threshold), illustrating that after 2 hours, a $^{19}$F signal clearly localizes in the stomach. D: corresponding $^{19}$F-MR image five hours after capsule administration (grey scale) that shows the absence of detectable localized signal, indicating the complete disintegration of the capsule and uptake of $^{19}$F-FDG. E: Non-localized $^{19}$F-NMR spectra acquired by a pulse-acquisition sequence from the abdominal region at the same 2 (lower spectrum) and 5 hour (upper spectrum) time points. The insert shows the quantification of the MR spectrum normalized to the signal at the two hour time point. These data illustrate that the total signal intensity of $^{19}$F-FDG inside the body has not changed. However, it is more dispersed, resulting in the absence of a localized $^{19}$F-MRI signal after 5 hours. The two $^{19}$F MR spectra were purposely shifted to enable better visualization and discrimination between the two spectra.

**Figure 4: CT of the capsule localized in the stomach.** Coated capsules containing $^{19}$F-FDG and $BaSO_4$ were administered to hamsters and subsequently visualized by CT. The stomach is filled with contrast agent six hours after administering the capsule. A: 2D projection image of a capsule (red arrow) right after administration, showing the intact capsule at the level of the stomach. B-D Reconstructed image 6 hours after administration of sagittal view (B), transverse view (C) and coronal view (D), illustrating the disintegration of the capsule inside the stomach. The red arrows indicate the location of the capsule inside the stomach, encircled in red in (C). The stomach content is hyperintense due to $BaSO_4$ released from the capsule.

**Figure 5: CT and MRI of the capsule localized in the small intestine.** Coated capsule containing $^{19}$F-FDG and $BaSO_4$ was localized (red arrow) in the small intestine 3 hours after administration. A: $^{19}$F-NMR spectrum shows the presence of $^{19}$F-FDG inside the body (arrow indicates the 19F peak). B-D: Reconstructed CT image of sagittal (B), transverse (C) and coronal view (D), demonstrating the presence of capsule remains and released $BaSO_4$ in the small bowel of the hamster.

## References


1. Gerding DN. Clostridium difficile infection prevention: biotherapeutics, immunologics, and vaccines. Discovery Medicine 2012; 13(68):75-83.
2. Magill SS, Edwards JR, Bamberg W, Beldavs ZG, Dumyati G, Kainer MA, Lynfield R, Maloney M, McAllister-Hollod L, Nadle J, Ray SM, Thompson DL, Wilson LE, Fridkin SK, Emerging Infections Program Healthcare-Associated I, Antimicrobial Use Prevalence Survey T. Multistate point-prevalence survey of health care-associated infections. The New England Journal of Medicine 2014; 370(13):1198-1208.
3. Louie TJ, Miller MA, Mullane KM, Weiss K, Lentnek A, Golan Y, Gorbach S, Sears P, Shue YK, Group OPTCS. Fidaxomicin versus vancomycin for Clostridium difficile infection. The New England Journal of Medicine 2011; 364(5):422-431.
4. Lowy I, Molrine DC, Leav BA, Blair BM, Baxter R, Gerding DN, Nichol G, Thomas WD, Jr., Leney M, Sloan S, Hay CA, Ambrosino DM. Treatment with monoclonal antibodies against Clostridium difficile toxins. The New England Journal of Medicine 2010; 362(3):197-205.
5. Giannasca PJ, Zhang ZX, Lei WD, Boden JA, Giel MA, Monath TP, Thomas WD, Jr. Serum antitoxin antibodies mediate systemic and mucosal protection from Clostridium difficile disease in hamsters. Infection and Immunity 1999; 67(2):527-538.
6. Ashford M, Fell JT. Targeting drugs to the colon: delivery systems for oral administration. Journal of Drug Targeting 1994;2(3):241-257.
7. Yang M, Cui F, You B, Wang L, Yue P, Kawashima Y. A novel pH-dependent gradient-release delivery system for nitrendipine II. Investigations of the factors affecting the release behaviors of the system. International Journal of Pharmaceutics 2004; 286(1-2):99-109.
8. Khan MZ, Prebeg Z, Kurjakovic N. A pH-dependent colon targeted oral drug delivery system using methacrylic acid copolymers. I. Manipulation Of drug release using Eudragit L100-55 and Eudragit S100 combinations. Journal of Controlled Release 1999; 58(2):215-222.

9. Matsumoto M, Kibe R, Ooga T, Aiba Y, Kurihara S, Sawaki E, Koga Y, Benno Y. Impact of intestinal microbiota on intestinal luminal metabolome. Scientific Reports 2012; 2:233.

10. Yoshida M, Kobayashi K, Kuo TT, Bry L, Glickman JN, Claypool SM, Kaser A, Nagaishi T, Higgins DE, Mizoguchi E, Wakatsuki Y, Roopenian DC, Mizoguchi A, Lencer WI, Blumberg RS. Neonatal Fc receptor for IgG regulates mucosal immune responses to luminal bacteria. The Journal of Clinical Investigation 2006; 116(8):2142-2151.

11. James ML, Gambhir SS. A molecular imaging primer: modalities, imaging agents, and applications. Physiological Reviews 2012; 92(2):897-965.

12. Goto T, Tanida N, Yoshinaga T, Sato S, Ball DJ, Wilding IR, Kobayashi E, Fujimura A. Pharmaceutical design of a novel colon-targeted delivery system using two-layer-coated tablets of three different pharmaceutical formulations, supported by clinical evidence in humans. Journal of Controlled Release 2004; 97(1):31-42.

13. Tuleu C, Khela MK, Evans DF, Jones BE, Nagata S, Basit AW. A scintigraphic investigation of the disintegration behaviour of capsules in fasting subjects: a comparison of hypromellose capsules containing carrageenan as a gelling agent and standard gelatin capsules. European Journal of Pharmaceutical Sciences 2007; 30(3-4):251-255.

14. Pedersen PB, Bar-Shalom D, Baldursdottir S, Vilmann P, Mullertz A. Feasibility of capsule endoscopy for direct imaging of drug delivery systems in the fasted upper-gastrointestinal tract. Pharmaceutical Research 2014; 31(8):2044-2053.

15. Christmann V, Rosenberg J, Seega J, Lehr CM. Simultaneous in vivo visualization and localization of solid oral dosage forms in the rat gastrointestinal tract by magnetic resonance imaging (MRI). Pharmaceutical Research 1997; 14(8):1066-1072.

16. Ai H. Layer-by-layer capsules for magnetic resonance imaging and drug delivery. Advanced Drug Delivery Reviews 2011; 63(9):772-788.

17. Himmelreich U, Dresselaers T. Cell labeling and tracking for experimental models using magnetic resonance imaging. Methods 2009; 48(2):112-124.

18. Terreno E, Castelli DD, Viale A, Aime S. Challenges for molecular magnetic resonance imaging. Chemical Reviews 2010; 110(5):3019-3042.
19. Nasongkla N, Bey E, Ren J, Ai H, Khemtong C, Guthi JS, Chin SF, Sherry AD, Boothman DA, Gao J. Multifunctional polymeric micelles as cancer-targeted, MRI-ultrasensitive drug delivery systems. Nano Letters 2006; 6(11):2427-2430.
20. Amiri H, Srinivas M, Veltien A, van Uden MJ, de Vries IJ, Heerschap A. Cell tracking using (19)F magnetic resonance imaging: technical aspects and challenges towards clinical applications. European Radiology 2015; 25(3):726-735.
21. Srinivas M, Heerschap A, Ahrens ET, Figdor CG, de Vries IJ. (19)F MRI for quantitative in vivo cell tracking. Trends in Biotechnology 2010; 28(7):363-370.
22. Nakada T, Kwee IL, Griffey BV, Griffey RH. 19F 2-FDG NMR imaging of the brain in rat. Magnetic Resonance Imaging 1988; 6(6):633-635.
23. Fidler JL, Fletcher JG, Bruining DH, Trenkner SW. Current status of CT, magnetic resonance, and barium in inflammatory bowel disease. Seminars in Roentgenology 2013; 48(3):234-244.
24. Saphier S, Rosner A, Brandeis R, Karton Y. Gastro intestinal tracking and gastric emptying of solid dosage forms in rats using X-ray imaging. International Journal of Pharmaceutics 2010; 388(1-2):190-195.
25. Krause W. Delivery of diagnostic agents in computed tomography. Advanced Drug Delivery Reviews 1999; 37(1-3):159-173.
26. Worsoe J, Fynne L, Gregersen T, Schlageter V, Christensen LA, Dahlerup JF, Rijkhoff NJ, Laurberg S, Krogh K. Gastric transit and small intestinal transit time and motility assessed by a magnet tracking system. BMC Gastroenterology 2011; 11:145.
27. Wempe MF, Buchanan CM, Buchanan NL, Edgar KJ, Hanley GA, Ramsey MG, Skotty JS, Rice PJ. Pharmacokinetics of letrozole in male and female rats: influence of complexation with hydroxybutenyl-beta cyclodextrin. The Journal of Pharmacy and Pharmacology 2007; 59(6):795-802.

28. Zhong J, Mills PH, Hitchens TK, Ahrens ET. Accelerated fluorine-19 MRI cell tracking using compressed sensing. Magnetic Resonance in Medicine 2013; 69(6):1683-1690.

29. Som P, Atkins HL, Bandoypadhyay D, Fowler JS, MacGregor RR, Matsui K, Oster ZH, Sacker DF, Shiue CY, Turner H, Wan CN, Wolf AP, Zabinski SV. A fluorinated glucose analog, 2-fluoro-2-deoxy-D-glucose (F-18): nontoxic tracer for rapid tumor detection. Journal of Nuclear Medicine 1980; 21(7):670-675.

30. Naressi A, Couturier C, Castang I, de Beer R, Graveron-Demilly D. Java-based graphical user interface for MRUI, a software package for quantitation of in vivo/medical magnetic resonance spectroscopy signals. Computers in Biology and Medicine 2001; 31(4):269-286.

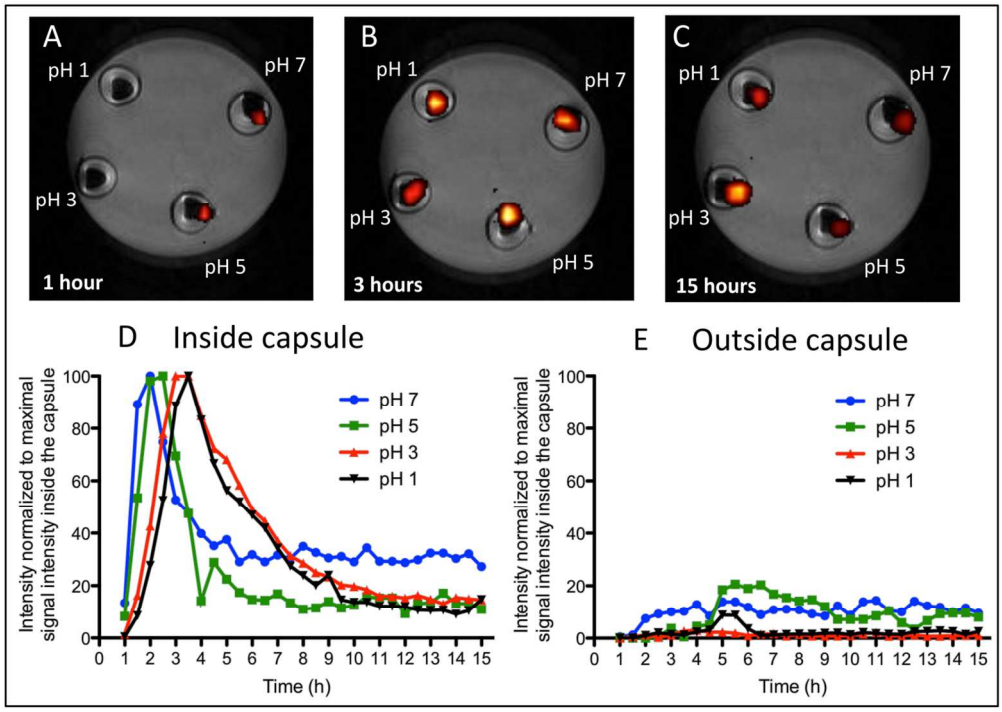


133x94mm (300 x 300 DPI)

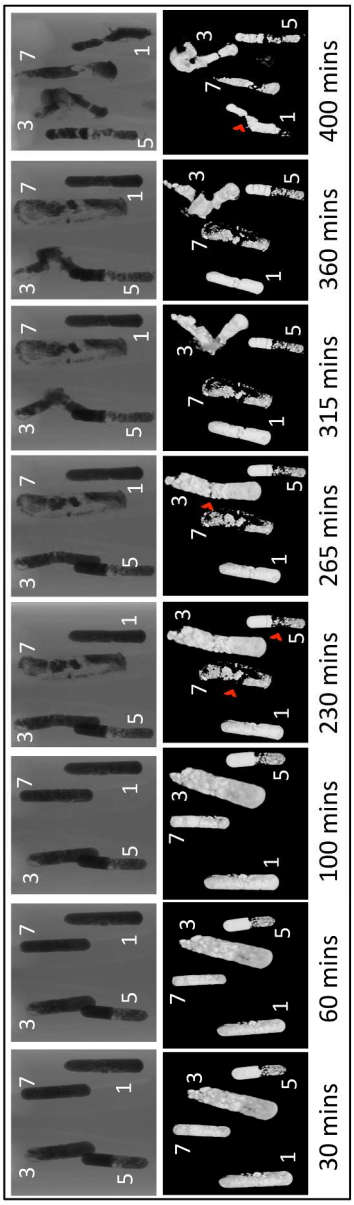


214x731mm (300 x 300 DPI)

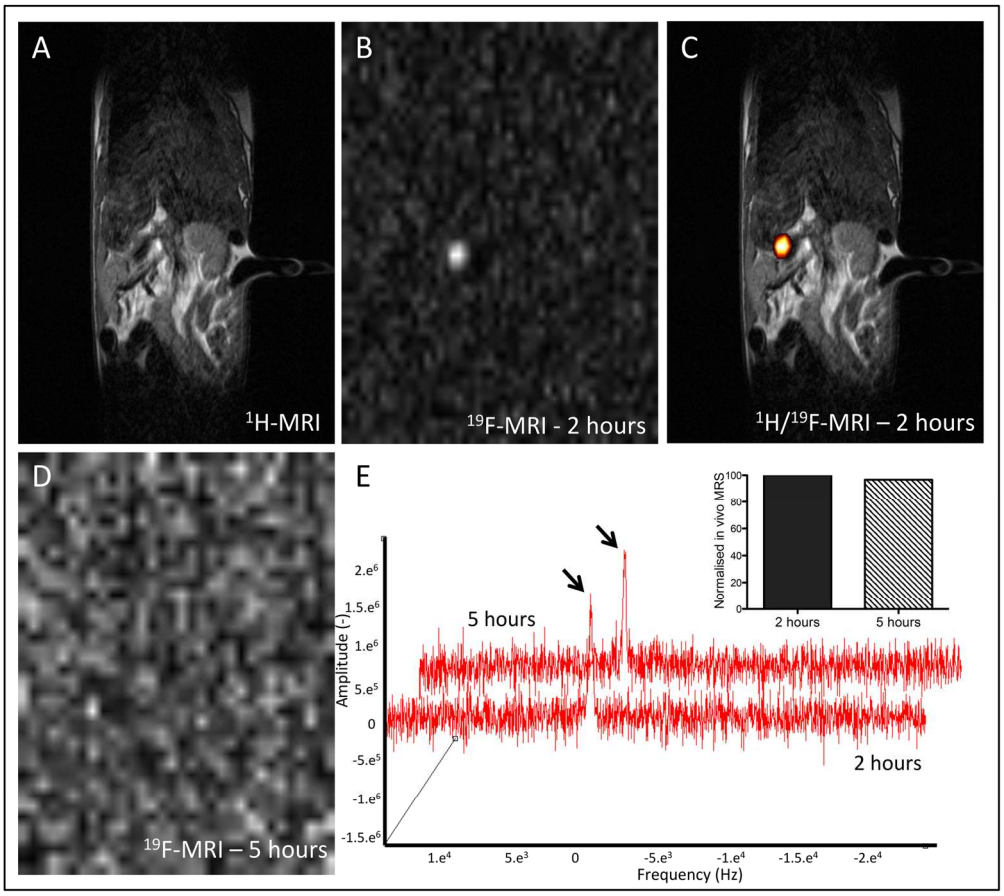


168x150mm (300 x 300 DPI)

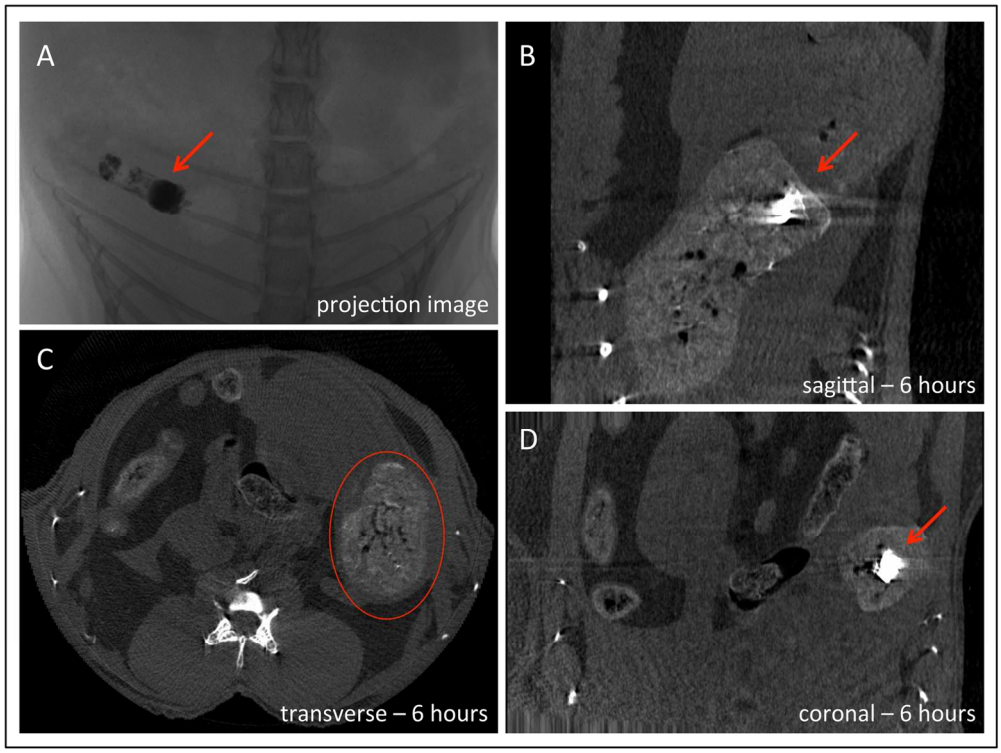


147x110mm (300 x 300 DPI)

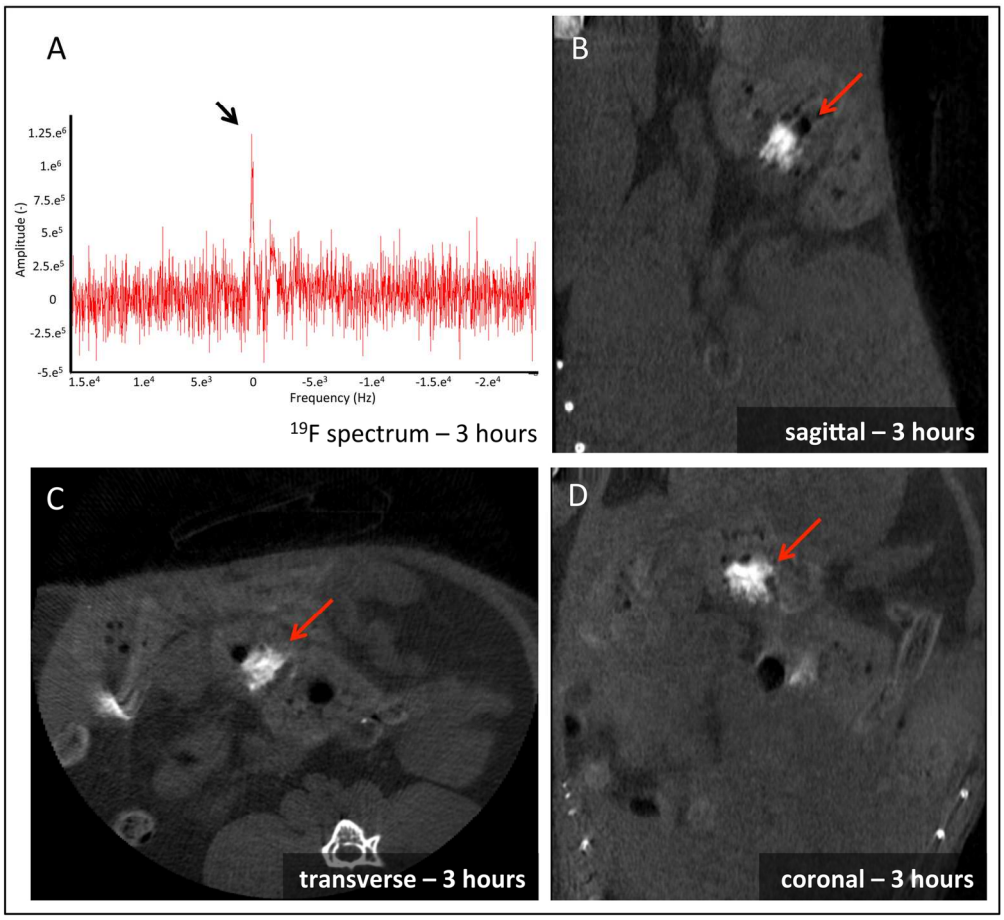


167x153mm (300 x 300 DPI)